Supplementary Information for

Decline of sediment transport due to damming and eco-engineering is approaching its limits

Boyan Li[1]✉, Yunchen Wang[2], Chao Wang[1], Wei Wang[1], Aiwen Lin[3], Gretchen C. Daily[4, 5]✉

[1] State Key Laboratory of Information Engineering in Surveying, Mapping and Remote Sensing, Wuhan University, Wuhan 430079, P.R. China.

[2] Shaanxi Satellite Application Technology Center for Natural Resources, Shaanxi Institute of Geological Survey, Xi'an 710054, P.R. China.

[3] School of Resources and Environmental Sciences, Wuhan University, Wuhan 430079, P.R. China.

[4] Stanford Woods Institute for the Environment, Stanford University, Stanford, California 94305, USA.

[5] Natural Capital Project, Stanford University, Stanford, California 94305, USA.

✉ e-mail: liboyan@whu.edu.cn(B. L.); gdaily@stanford.edu(G.C.D.)

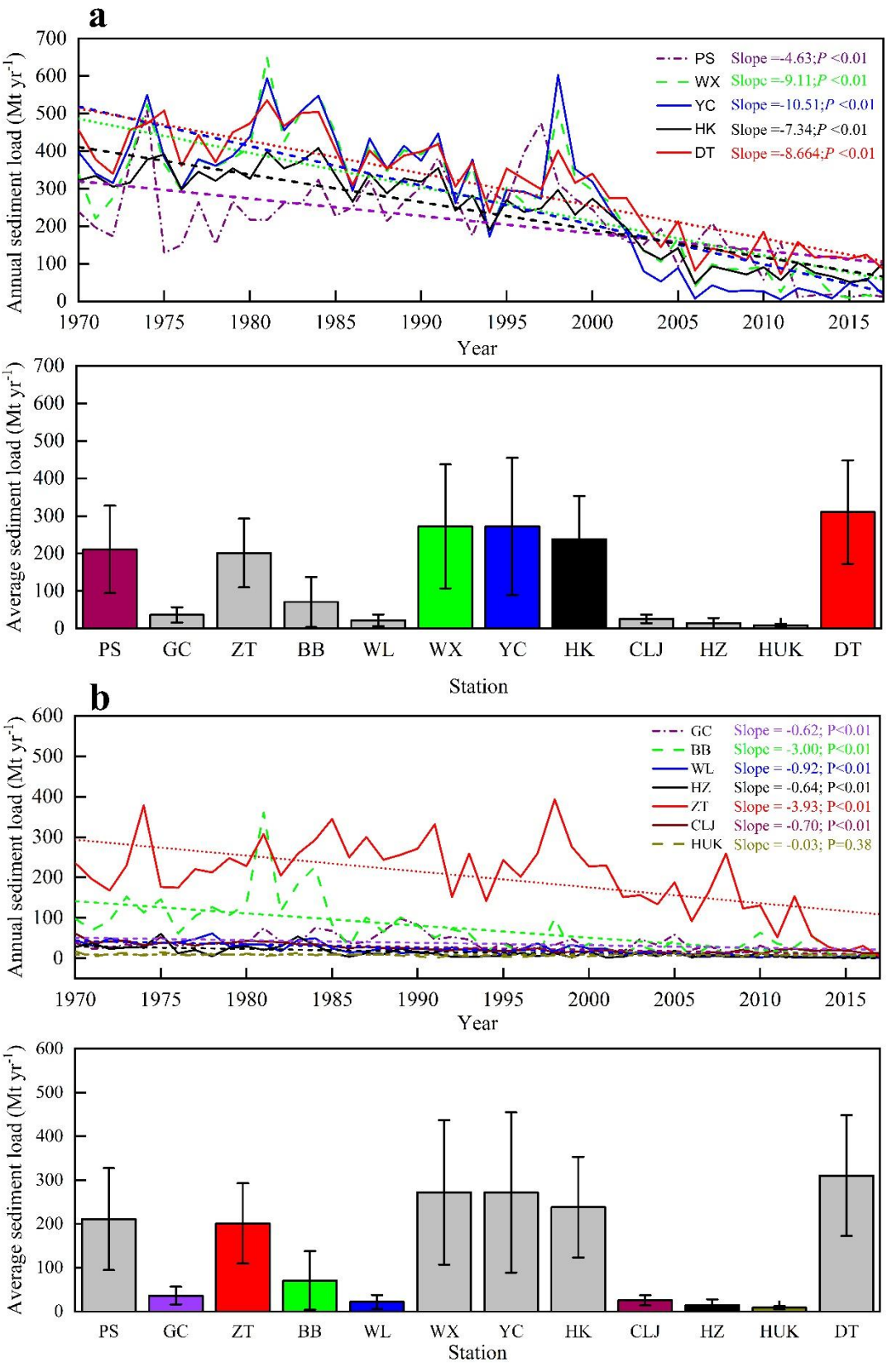
a
Annual sediment load (Mt yr-1)
Year
PS Slope =-4.63;P <0.01
WX Slope =-9.11;P <0.01
YC Slope =-10.51;P <0.01
HK Slope =-7.34;P <0.01
DT Slope =-8.664;P <0.01
Average sediment load (Mt yr-1)
PS GC ZT BB WL WX YC HK CLJ HZ HUK DT
Station
b
Annual sediment load (Mt yr-1)
Year
GC Slope = -0.62; P<0.01
BB Slope = -3.00; P<0.01
WL Slope = -0.92; P<0.01
HZ Slope = -0.64; P<0.01
ZT Slope = -3.93; P<0.01
CLJ Slope = -0.70; P<0.01
HUK Slope = -0.03; P=0.38
Average sediment load (Mt yr-1)
PS GC ZT BB WL WX YC HK CLJ HZ HUK DT
Station

21

Supplementary Figure 1. The hydrologic regime of the Yangtze River during 1972-2016. Dashed lines represent trend lines of the sediment load. Error bars are the standard deviation across the years. The annual load shows a significant reduction during these periods. **a**: time series of annual sediment load at the main gauging stations along the mainstream of the Yangtze River(top). The average annual sediment load from 1972 to 2016 at gauging stations(bottom); **b**: time series of annual sediment load at the seven gauging stations along the main tributaries (except ZT station) of the Yangtze River(top). The average annual sediment load from 1970 to 2017 at gauging stations(bottom), error bars are the standard deviation across the years. PS, Pingshan; GC, Gaochang; ZT, Zhuotuo; BB, Beibei; WL,Wulong; WX, Wanxian; YC,Yichang; HK, Hankou; CLJ, Chenglingji; HZ, Huangzhuang; HUK, Hukou; DT, Datong.

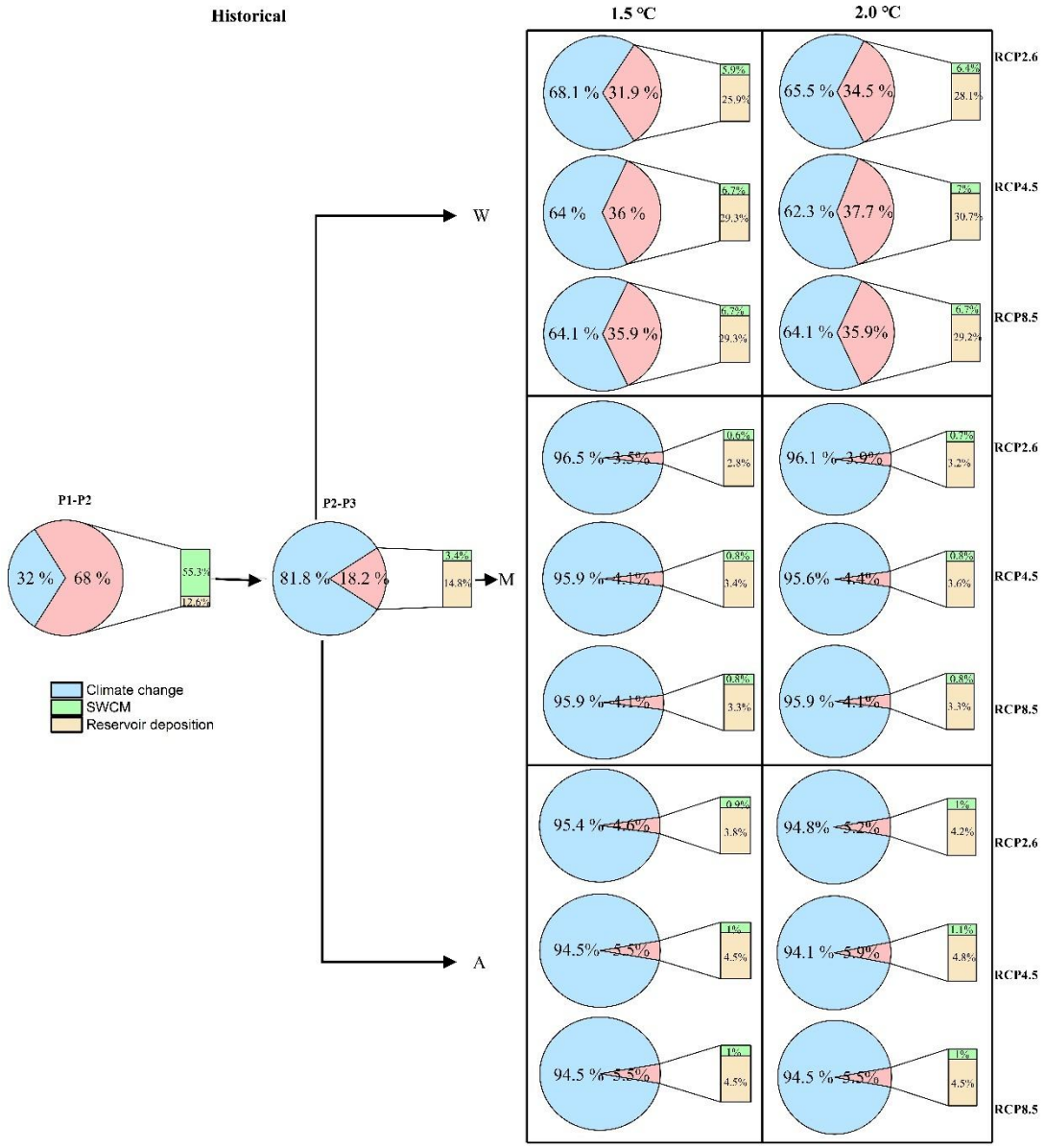

Supplementary Figure 2. Relative contributions of climate change and human activities (i.e., reservoir deposition and SWCM) to sediment load change in historical period (the difference between PZH and DT stations) (left). We assume that the relative contribution of reservoir deposition and SWCM in human activities to sediment transport under historical and future scenarios remains unchanged. Projected the relative contributions of climate change and human activities (including reservoir deposition and SWCM) by multimodel mean in each of

the three scenarios (W scenario, M scenario, A scenario) for the 1.5 °C and 2.0 °C warming scenarios (corresponding to periods of 2020–2039 and 2040–2059, respectively) relative to the reference period (1972–1992) (right). The significance of the changes was tested with the two-sample t test at the 0.05 significance level. PZH, Panzhihua; DT, Datong; SWCM, Soil and water conservation measures.

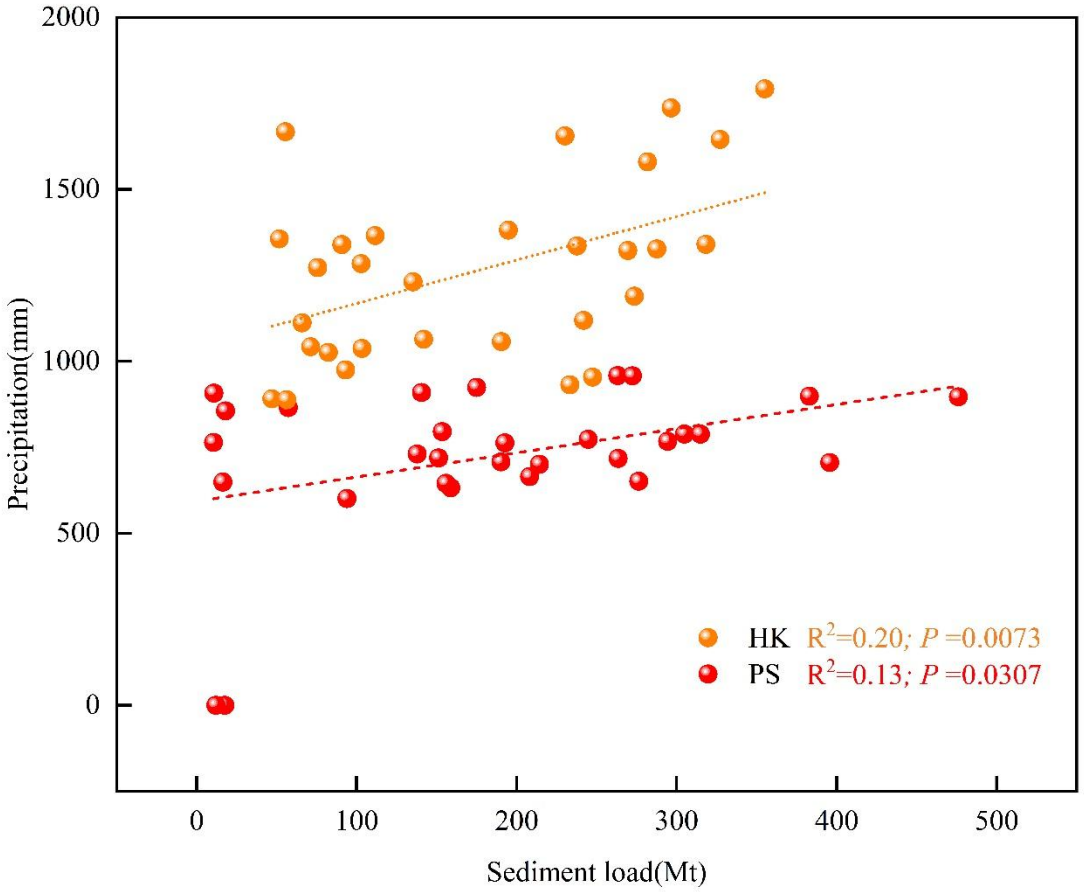

Supplementary Figure 3. Relationship between precipitation and sediment load [coefficient of determination (R^2); significance (P)]. According to the observational data, we selected the annual precipitation (mm) and sediment load data of PS Station and HK Station to calculate the relationship between precipitation and sediment load. These hydrological data were quality controlled at the office of the Hydrological Bureau of the Yangtze River Water

Resources Commission in Wuhan, China. HK, Hankou; PS, Pingshan.

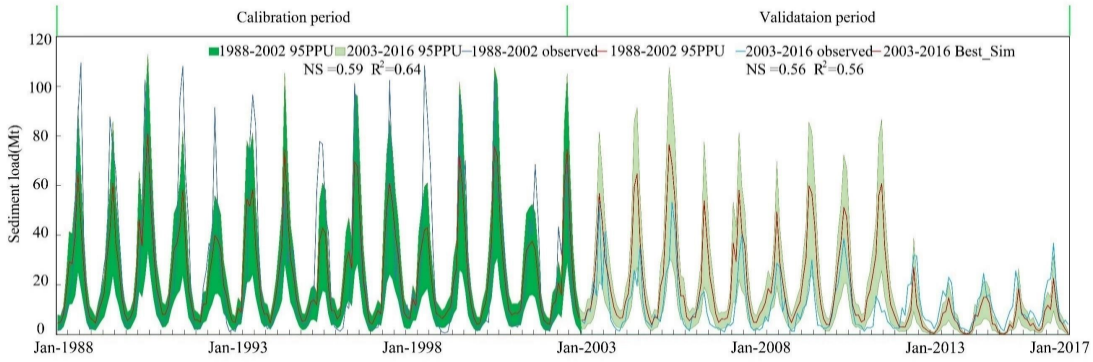

Supplementary Figure 4. Comparison of simulated and observed values and model evaluation results. R^2 and NS represent the coefficient of determination, Nash-Sutcliffe efficiency, respectively. The calibration period is 1988–2002, and the validation period is 2003–2016.

Supplementary Table 1. The relative contribution of climate changes and human activities to annual runoff in the YRB during the period P1–P2, P2–P3 and P1–P3.

	P1- P2					P2- P3					P1- P3				
	Climate change		Human activities		Change	Climate change		Human activities		Change	Climate change		Human activities		Change
	CC_1 HA_1	CC_2 HA_1	CC_1 HA_2	CC_2 HA_2		CC_2 HA_2	CC_3 HA_2	CC_2 HA_3	CC_3 HA_3		CC_1 HA_1	CC_3 HA_1	CC_1 HA_3	CC_3 HA_3	
Observed sediment load (Mt)	422.1			515	22.0%	309			131.6	-57.4 %	422.1			131.6	-68.8 %
Simulated sediment load (Mt)	416.1	433.3	396.8	478.6	15.0%	483.4	1514	409.3	176.6	-63.5 %	416.1	142.0	403.5	176.6	-57.6 %
Change in simulated sediment load (Mt)		17.2	-36.4	62.5	81.8		-332.0	-74.1	-306.8	99.3		-274.1	-12.6	-239.50	47.3
Relative contribution (%)		27.5	58.3	100.0	-14.3		108.2	24.1	100.0	32.4		114.5	5.3	100.0	19.7
Normalization of relative contribution (%)		32.04	67.96				81.76	18.24				95.60	4.40		

Notes: CC_1 and HA_1 denotes the baseline period (P1) of climate change scenario and human activity scenario, respectively. We followed the same naming rule to denote the other climate change scenario and human activity scenario.

Supplementary Table 2. The area of imperious surface equivalent (S_{ISE}) and the intensity of ecological engineering (IEE) in the study site from 1988 to 2016, and three scenarios to 2050 (Unit: $\times 10^6$ ha)

Year	Cropland	Forest	Grassland	Unused land	Urban land	Water body	S_{ISE}	IEE
1988	50.44	72.89	41.48	5.13	2.34	5.89	24.6608	13.8420
1989	50.36	72.78	41.49	5.06	2.38	6.08	24.6787	13.8520
1990	50.36	72.78	41.49	5.06	2.38	6.08	24.6787	13.8520
1991	50.36	72.78	41.49	5.06	2.38	6.08	24.6787	13.8521
1992	50.36	72.78	41.49	5.06	2.38	6.08	24.6787	13.8520
1993	49.64	73.27	42.64	4.88	2.60	5.13	24.9277	13.9918
1994	49.64	73.27	42.64	4.88	2.61	5.13	24.9293	13.9927
1995	49.59	73.32	42.66	4.87	2.61	5.11	24.9321	13.9942
1996	49.59	73.32	42.66	4.87	2.61	5.11	24.9321	13.9942
1997	49.59	73.32	42.66	4.87	2.61	5.11	24.9322	13.9943
1998	49.92	72.80	41.69	5.13	2.79	5.84	25.0203	14.0438
1999	49.92	72.80	41.69	5.13	2.79	5.84	25.0202	14.0437
2000	49.92	72.80	41.69	5.13	2.79	5.84	25.0202	14.0437
2001	49.89	72.80	41.68	5.14	2.80	5.84	25.0288	14.0486
2002	49.78	72.82	41.67	5.17	2.89	5.83	25.0946	14.0855
2003	49.56	72.88	41.63	5.23	3.05	5.81	25.2161	14.1537
2004	49.47	72.89	41.63	5.25	3.11	5.81	25.2554	14.1757
2005	49.41	72.90	41.62	5.27	3.14	5.81	25.2804	14.1898
2006	49.40	72.90	41.62	5.27	3.16	5.81	25.2915	14.1960
2007	49.34	72.91	41.61	5.28	3.21	5.81	25.3327	14.2191
2008	49.12	72.93	41.58	5.29	3.41	5.82	25.4917	14.3084
2009	49.09	72.93	41.58	5.30	3.44	5.82	25.5153	14.3216
2010	49.06	72.94	41.57	5.30	3.47	5.82	25.5378	14.3342
2011	49.02	72.93	41.57	5.30	3.52	5.82	25.5739	14.3545
2012	48.97	72.92	41.57	5.31	3.58	5.82	25.6245	14.3829
2013	48.61	72.79	41.56	5.35	4.03	5.82	25.9906	14.5884
2014	48.51	72.76	41.56	5.36	4.15	5.82	26.0872	14.6426
2015	48.43	72.73	41.56	5.37	4.25	5.82	26.1695	14.6888
2016	48.30	72.82	41.55	5.39	4.39	5.71	26.2872	14.7549
W scenario	48.04	73.07	40.04	6.01	5.99	5.00	27.7131	15.5565
M scenario	49.04	74.07	37.03	6.01	6.99	5.00	28.7243	16.1242
A scenario	49.05	70.06	40.16	5.57	9.01	4.29	30.6108	17.1831

Note: For details, please refer to literature[1,2].

Supplementary Table 3. The scenario setting of this study.

Scenario	Factor		Group
	Weather data	Land use	
H1	CC_1	HA_1	Historical
H2	CC_2	HA_1	
H3	CC_1	HA_2	
H4	CC_2	HA_2	
H5	CC_3	HA_2	
H6	CC_2	HA_3	
H7	CC_3	HA_1	
H8	CC_1	HA_3	
H9	CC_3	HA_3	
S1	The baseline period (1972-1992)	W	HadGEM2-ES
S2	The baseline period (1972-1992)	M	
S3	The baseline period (1972-1992)	A	
S4	The baseline period (1972-1992)	LULC(1990)	
S5	RCP2.6(2017-2059)	W	
S6	RCP2.6(2017-2059)	M	
S7	RCP2.6(2017-2059)	A	
S8	RCP2.6(2017-2059)	LULC(1990)	
S9	RCP4.5(2017-2059)	W	
S10	RCP4.5(2017-2059)	M	
S11	RCP4.5(2017-2059)	A	
S12	RCP4.5(2017-2059)	LULC(1990)	
S13	RCP8.5(2017-2059)	W	
S14	RCP8.5(2017-2059)	M	
S15	RCP8.5(2017-2059)	A	
S16	RCP8.5((2017-2059)	LULC(1990)	
S17	RCP2.6(2017-2059)	W	IPSL-CM5A-LR
S18	RCP2.6(2017-2059)	M	
S19	RCP2.6(2017-2059)	A	
S20	RCP2.6(2017-2059)	LULC(1990)	
S21	RCP4.5(2017-2059)	W	
S22	RCP4.5(2017-2059)	M	
S23	RCP4.5(2017-2059)	A	
S24	RCP4.5(2017-2059)	LULC(1990)	
S25	RCP8.5(2017-2059)	W	
S26	RCP8.5(2017-2059)	M	
S27	RCP8.5(2017-2059)	A	
S28	RCP8.5((2017-2059)	LULC(1990)	
S29	RCP2.6(2017-2059)	W	IPSL-CM5A-MR
S30	RCP2.6(2017-2059)	M	
S31	RCP2.6(2017-2059)	A	
S32	RCP2.6(2017-2059)	LULC(1990)	
S33	RCP4.5(2017-2059)	W	
S34	RCP4.5(2017-2059)	M	
S35	RCP4.5(2017-2059)	A	
S36	RCP4.5(2017-2059)	LULC(1990)	
S37	RCP8.5(2017-2059)	W	
S38	RCP8.5(2017-2059)	M	
S39	RCP8.5(2017-2059)	A	
S40	RCP8.5((2017-2059)	LULC(1990)	

Notes: LULC (1990) represent the land use and cover maps in 1990.

Supplementary Table 4. SWAT parameters used to calibrate YRB hydrologic model

Parameter	Range of values	Mean value (SD)	Units	Description
r__CN2.mgt	-1~1	0.5(0.35)	na	Curve number
r__SOL_AWC().sol	-1~1	0.03(0.58)	mm/mm	Available soil water capacity
r__GWQMN.gw	-1~1	0.6(0.66)	mm H2O	Threshold depth of water in the shallow aquifer required for return flow to occur
r__GW_REVAP.gw	-1~1	-0.27(0.67)	na	Groundwater "revap" coefficient
r__SLSUBBSN.hru	-1~1	0.09(0.63)	m	Average slope length
r__SURLAG.bsn	-1~1	-0.33(0.57)	na	Surface runoff lag coefficient
r__CANMX.hru	-1~1	-0.06(0.55)	mm H_2O	Maximum canopy storage
r__SOL_K().sol	-1~1	0.09(0.37)	na	USLE equation soil erodibility (K) factor.
r__USLE_P.mgt	-1~1	0.26(0.48)	na	USLE equation support pra
v__ALPHA_BF.gw	0~1	0.45(0.37)	days	Base flow alpha factor or recession constant
v__GW_DELAY.gw	0~500	85.69 (72.28)	days	Groundwater delay
v__CH_N2.rte	-0.01~0.3	0.15 (0.05)	na	Channel mannings roughness coefficient
v__CH_K2.rte	-0.01~500	323.12 (57.93)	mm/hr	Channel hydraulic conductivity
v__EPCO.hru	0~1	0.33(0.31)	na	Plant uptake compensation factor
v__ESCO.hru	0~1	0.71(0.25)	na	Soil evaporation compensation factor
v__SPCON.bsn	0.0001~0.01	0.002(0.001)	na	Linear parameter for calculating the maximum amount of sediment that can be reentrained during channel sediment routing.
v__SPEXP.bsn	1~1.5	1.27(0.04)	na	Exponent parameter for calculating sediment reentrained in channel sediment routing.
v__REVAPMN.gw	0~500	339.72 (142.14)	mm H_2O	Threshold depth of water in shallow aquifer for "revap" or percolation to deep aquifer to occur

Note: Range of values was applied to 10 individual subbasins that compose the YRB hydrologic model. Mean (SD) values are based on SWAT best parameter values for the10 individual subbasins. X_Code indicate the type of change to be applied to the parameter, v_ means the existing parameter value is to be replaced by the given value, and r_means the existing parameter value is multiplied by (1+a given value).

Supplementary Table 5. Performance metrics of simulated sediment on the YRB for

the calibration, validation, and overall periods, respectively.

Time period		Climate change	Human activities	NS	R^2
H0	Calibration (1972~2003)	/	/	0.59	0.64
	Validation (2004~2016)	/	/	0.56	0.56
H1 (natural period)	Calibration (1972~1993)	CC_1	HA_1	0.73	0.73
	Validation (1994~1998)	/	/	0.59	0.64
H2	Calibration (1994~2003)	CC_2	HA_1	0.65	0.62
	Validation (2004~2008)	/	/	0.59	0.61
H3	Calibration (1972~1993)	CC_1	HA_2	0.73	0.73
	Validation (1994~1998)	/	/	0.74	0.74
H4	Calibration (1994~2003)	CC_2	HA_2	0.65	0.62
	Validation (2004~2008)	/	/	0.57	0.60
H5	Calibration (2004~2014)	CC_3	HA_2	0.66	0.66
	Validation (2015~2016)	/	/	0.62	0.58
H6	Calibration (1994~2003)	CC_2	HA_3	0.65	0.62
	Validation (2004~2008)	/	/	0.57	0.60
H7	Calibration (1972~1993)	CC_1	HA_3	0.69	0.59
	Validation (1994~1998)	/	/	0.68	0.55
H8	Calibration (2004~2014)	CC_3	HA_1	0.73	0.74
	Validation (2015~2016)	/	/	0.69	0.60
H9	Calibration (2004~2014)	CC_3	HA_3	0.70	0.59
	Validation (2015~2016)	/	/	0.68	0.58

Notes: Bold number indicates an unsatisfactory fit. According to ref [3], NS = 1.0 is the perfect fit, NS > 0.75 is a very good fit, NS = 0.64 to 0.74 is a good fit, NS = 0.5 to 0.64 is a satisfactory fit and NS < 0.5 is an unsatisfactory fit.

S1 Breakpoints and trend analysis of annual sediment load.

The breaks for additive season and trend (BFAST) algorithm (Sections S7) and the Mann-Kendall method (Sections S8) was applied for breakpoints and trend analysis of runoff. As seen in Supplementary Figure 1, twelve hydrological stations exhibited a significant downward trend, whereas HUK station shown a non-significant decreasing

trend. The change points were detected for all twelve gauging stations, most of them occurring in the period of 1990-1993, 1998, and 2000–2003 (Fig. 2 and Supplementary Figure 5). The whole study period was split into three sub-periods (1972–1992, 1993–2003, 2004–2016) to quantify the change in sediment load.

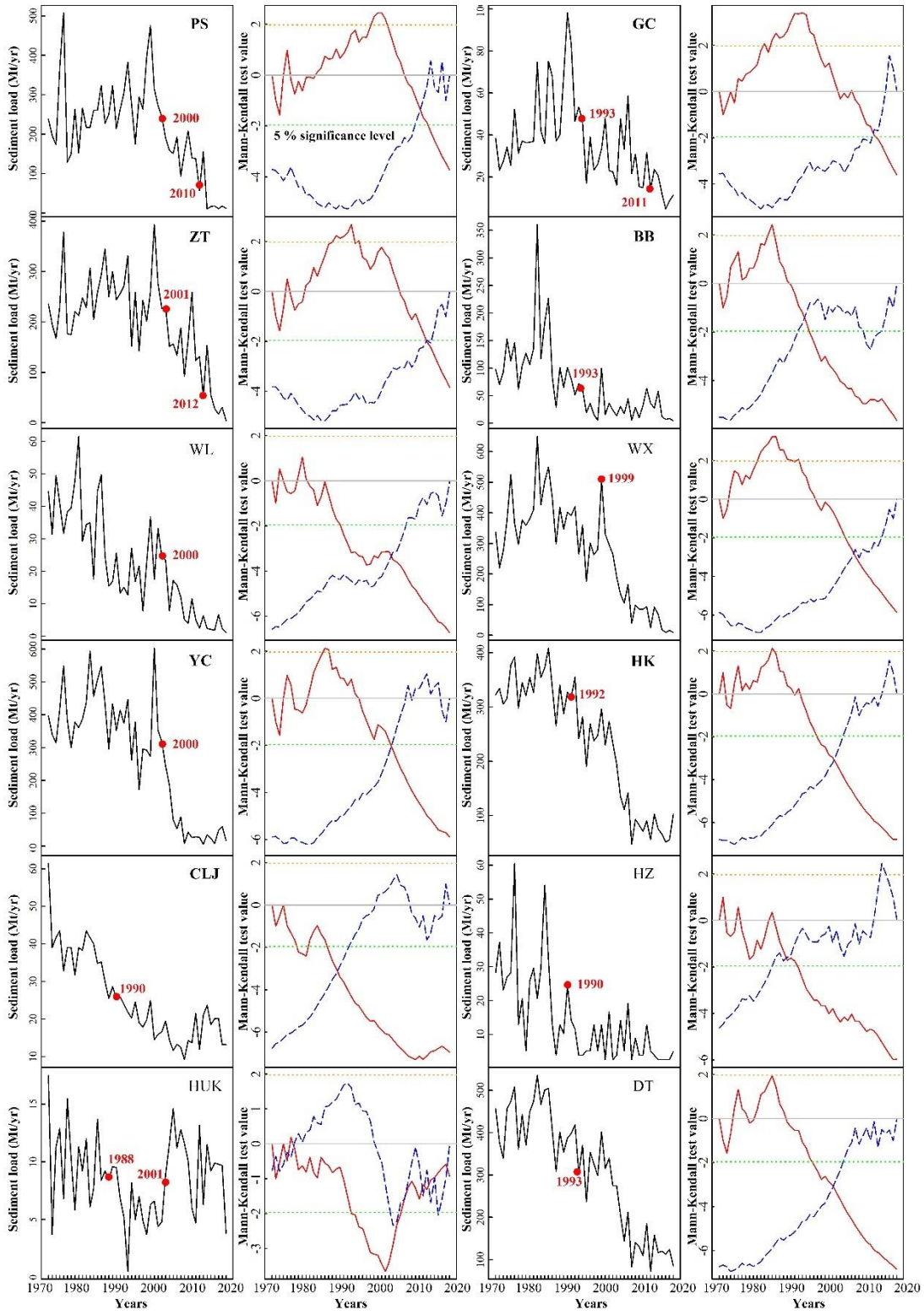

Supplementary Figure 5. Abrupt change points in sediment load estimated by Pettitt test and Mann-Kendall test in selected sub-basins of YRB. Horizontal dashed lines represent

significance at 5 % significance level. The blue and red solid lines represent the progressive series, UF, and the retrograde series, UB. For subbasins with abrupt changes in the sediment transport, the larger red points represent abrupt change point illustrated by Pettitt test and Mann-Kendall test (refer to section S4).

S2 Climate model selection

In this study, future characteristics of temperature and precipitation impacts are analyzed over the Yangtze River Basin with nine global climate models (GCMs) in CMIP5 (Coupled Model Intercomparison Project phase 5) (Supplementary Table 7): HadGEM2-ES, MPI-ESM-LR, MPI-ESM-MR. Three representative concentration pathways (RCPs) are considered, i.e., RCP2.6, RCP4.5 and RCP8.5. Using a multimodel mean, projections for 20-y intervals were estimated when the average global warming reaches the 1.5 °C thresholds under RCP2. 6 and the 2.0 °C thresholds under RCP4.5[4]. It is estimated that the 2.0 °C warming threshold would be reached in 2020–2039 under RCP2.6 and the 2.0 °C warming threshold would be reached in 2040–2059 under RCP4.5[4,5].

Supplementary Table 6. Statistical comparison of observed temperature and precipitation with 24 GCMs over the Yangtze River Basin the period of 1960-2005[6]. Altogether 24 simulations from nine models are found to meet the research requirement for calculation of temperature and precipitation for future period under RCP2.6, RCP4.5 and RCP8.5 scenarios. AE, RE and NRMSE is the absolute error, relative error and normalized root mean square error, respectively.

NO.	Climate model	Temperature	Precipitation

		AE(%)	NRMSE(%)	Selected	RE(%)	NRMSE(%)	Selected
1	BCC-CSM1.1	0.38	1.22		3	1.52	
2	BNU-ESM	-0.80	1.22		48	1.64	
3	CanESM2	-0.50	1.14		29	1.53	
4	CCSM4	-2.02	1.13		31	1.60	
5	CNRM-CM5	-1.31	1.14		43	1.68	
6	CSIRO-MK3.6.0	0.10	1.23		31	1.55	
7	FGOALS-g2	-2.82	1.24		32	1.63	
8	FIO-ESM	-0.79	1.22		43	1.51	
9	GFDL-CM3	-3.43	1.15		24	1.49	
10	GFDL-ESM2G	-2.83	1.15		25	1.56	
11	GISS-E2-H	-1.60	1.17		33	1.65	
12	GISS-E2-R	-1.80	1.15		41	1.69	
13	HadGEM2-AO	-0.48	1.14		41	1.76	
14	HadGEM2-ES	-1.33	1.12	√	18	1.30	√
15	IPSL-CM5A-LR	-1.34	1.27		14	1.40	√
16	IPSL-CM5A-MR	-2.13	1.19		10	1.37	√
17	MIROC5	-1.24	1.26		41	1.72	
18	MIROC-ESM	-0.47	1.21		26	1.68	
19	MIROC-ESM-CHEM	-0.54	1.21		29	1.68	
20	MPI-ESM-LR	-0.61	1.17		34	1.55	
21	MPI-ESM-MR	-0.65	1.15		25	1.45	
22	MRI-CGCM3	-1.92	1.15		40	1.63	
23	NorESM1-M	-1.83	1.14		24	1.48	
24	NorESM1-ME	-1.87	1.15		28	1.50	

S3 Method for Mapping Land Use Biomes for Future Scenarios and regional implications

Our approach to developing representations of regional land use/cover for each of the three scenarios (Weak (W), Moderate (M), and Ambitious (A)) was based on an initial regional land cover product, henceforth referred to as the 2016 Land Use Base Map or Base_2016 for short (Supplementary Figure 7). Base_2016 was the initial 2016 base land use dataset used in the algorithm to produce the land use maps for the four scenarios to 2050 (Supplementary Table 2). The algorithm was driven by the percent

changes to regional total biome areas. The algorithm distributes these percent changes over the surface of the planet. Base_2016 and all three scenarios were prepared in an equal area Albers projection. From this dataset, we created binary layers for each biome (e.g. urban was assigned 1, everything else was assigned a 0 or NoData) and we combined all cropland into one cropland category, all forest land (e.g. woodland, shrub land, sparse woodland) into one forest land category, all grassland (e.g. high-coverage grassland, medium-coverage grassland, low-coverage grassland) into one grassland category, and all unused land (e.g. sandy land, saline alkali land and bare soil) into one unused land category (Supplementary Figure 6). All water categories (e.g. rivers, lakes, reservoirs) were assigned to an excluded layer, which prevented them from undergoing any transitions. In addition, we created a global grid of random numbers drawn from a uniform distribution ranging from 1 to 100 for every terrestrial pixel, with ocean areas set at 0 (Rnd_Water_0) (Supplementary Figure 6). The approach permits growth or shrinkage of each of the remaining biomes (urban, cropland, forest, grassland, and unused land) by the set percentages (Supplementary Table 1) to produce the land cover changes seen in the three scenarios. The precedence of land cover transitions was as follows:

1) Grew urban extent from existing urban pixels. This growth was permitted to consume all the other biomes not in the excluded layer. (Note: All urban pixels were excluded from future transitions.)

2) Grew or shrank croplands from remaining croplands. Ensured that the percentage growth or loss was relative to original extent of croplands prior to previous

143 land cover transitions. (Note: At this point both urban and cropland were excluded
144 from future transitions.)

145 3) Grew or shrank forest land from remaining forest land. Ensured that the
146 percentage of growth or loss was relative to original extent of forest land prior to
147 previous land cover transitions. (Note: Forest land now became an excluded layer.)

148 4) Grew or shrank grassland from remaining grassland. Ensured that the
149 percentage growth or loss was relative to original extent of grassland prior to previous
150 land cover transitions. In cases of grassland losses, unused land became grasslands.
151 (Note: Grassland now became an excluded layer.)

152 5) Grew or shrank unused land from remaining unused land. This was done so
153 that the final areal extent of unused land was the correct percentage change relative to
154 original extent of unused land.

155 We were then able to recombine the new land cover extents into one regional
156 coverage map for each scenario. For detailed information, please refer to the
157 literature[7]. We followed the same procedures to produce the other three scenarios and
158 then got geotiffs datasets of Base_2016, W_Scenario, M_Scenario, and A_Scenario to
159 2050 (Supplementary Figure 7).

160 **Supplementary Table 7.** Three scenarios original changes with land use percent changes

Scenarios	**1980**	**2016**	**Scenarios to 2050**		
			W	**M**	**A**
			Weak	Moderate	Ambitious
Total Area (e6 ha)	**~178**				
Cropland（e6 ha）	51	48	48	49	55
Forest land（e6 ha）	73	73	73	74	77
Grassland（e6 ha）	41	41	40	37	28
Water bodies（e6 ha）	5	6	6	6	6
Urban land（e6 ha）	2	5	6	7	9

Unused land （e6 ha）	6	5	5	5	3
Percent Changes （%）					
Cropland	28.42	26.73	0.24	0.80	4.17
Forest land	40.98	41.17	-0.16	0.41	2.09
Grassland	23.27	23.03	-0.56	-2.25	-7.30
Water bodies	2.93	3.13	0.00	0.00	0.00
Urban land	1.28	3.00	0.37	0.94	2.06
Unused land	3.20	2.99	-0.18	-0.18	-1.31

Notes: the colours of the numbers indicate: black values are values that have remained constant, green are values that have increased, red are values that have decreased from the 2016 values.

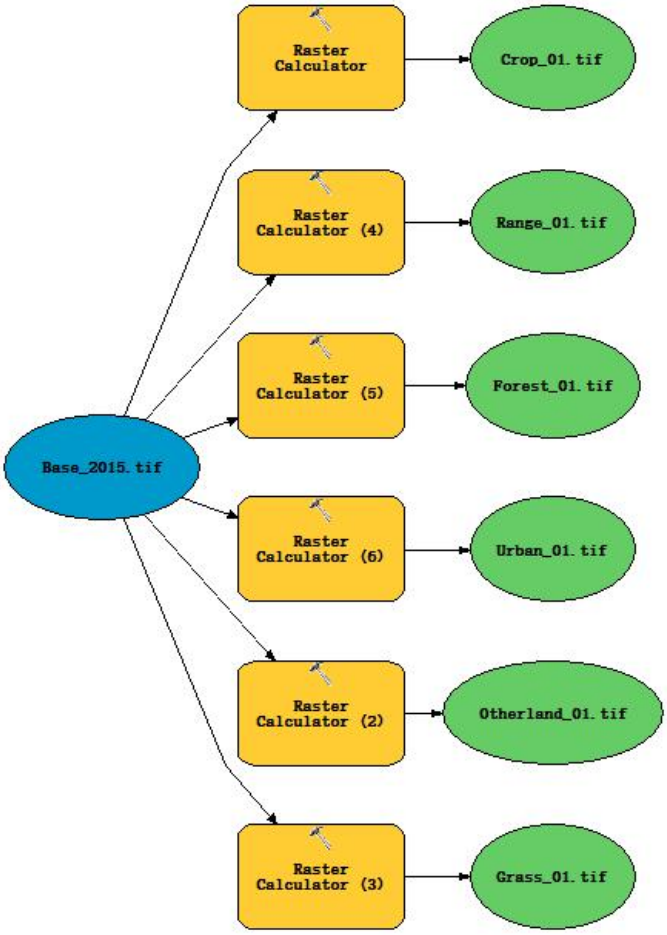

Supplementary Figure 6. Creation of Binary Biome Data Layers (ArcGIS Model Builder)

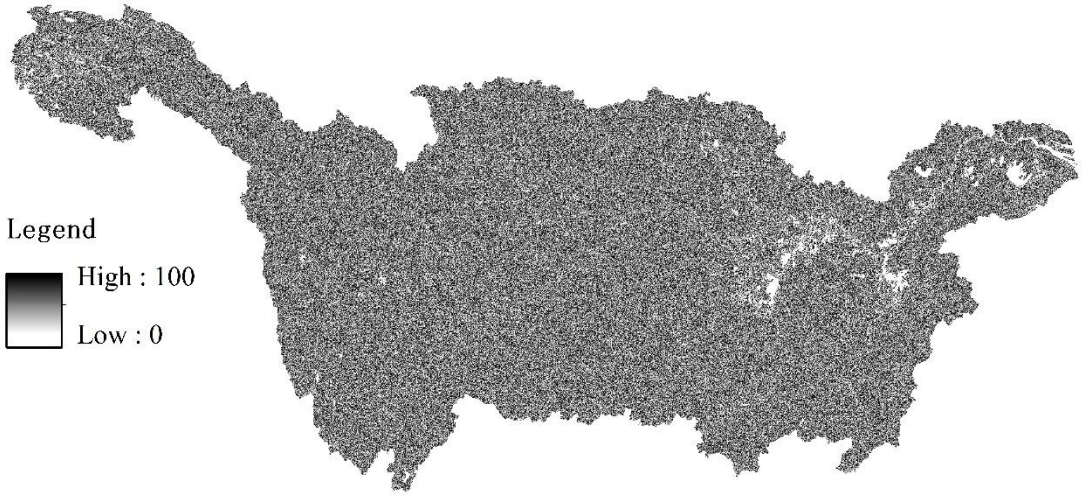

166

167 **Supplementary Figure 7.** Randomized Terrestrial Layer used to partition selections

168 (Rnd_Water_0). Mask of Rnd_Water_0 was performed using the "Extract by Mask" tool in

169 ArcGIS software Version10.2.

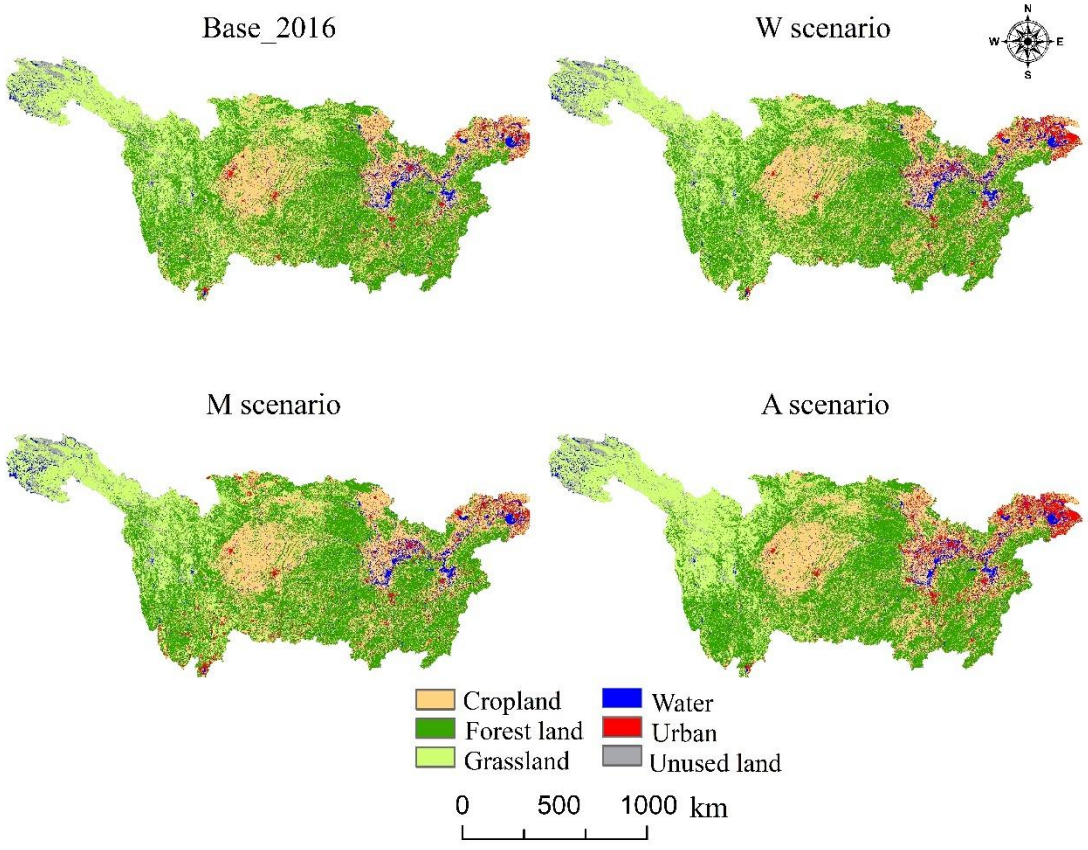

170

Supplementary Figure 8. Four land use maps of the YRB showing the 2016 labeled Base and the land use maps of the YRB for each of the scenarios (labeled Scenario W, M, and A).

S4 Mann-Kendall (MK) trend test

The non-parametric (M-K) trend test was used to detect both the trends and abrupt changes in hydrometeorological time series [8–12]。For a time series $x_t = (x_1, x_2, \cdots, x_n)$, the standardized test statistic Z is given as:

$$Z = \begin{cases} (S-1)/\sqrt{\mathrm{var}(S)} & S > 0 \\ 0 & S = 0 \\ (S+1)/\sqrt{\mathrm{var}(S)} & S < 0 \end{cases} \quad (1)$$

in which

$$S = \sum_{j=1}^{n-1} \sum_{k=j+1}^{n} \mathrm{sgn}(x_k - x_j) = \begin{cases} 1 & x_k - x_j > 0 \\ 0 & x_k - x_j = 0 \\ -1 & x_k - x_j < 0 \end{cases} \quad (2)$$

$$\mathrm{var}(S) = \left[n(n-1)(2n+5) - \sum_{t}^{p} q_t(q_t-1)(2q_t+5) \right] / 18 \quad (3)$$

$$\beta = \mathrm{median}\left[(x_k - x_j)/(k-j) \right] \quad 1 < j < k < n \quad (4)$$

where S is the test statistic value, n is the length of the sample, x_k and x_j are from $j=1,2,\cdots,n-1$ and $k=j+1, j+2,\cdots,n$ ($k > j$), respectively, p is the total number of tie groups in the data, and q_t is the number of data points contained in the t-th tie group; β is Sen's slope estimate, $\beta>0$ indicates upward trend in a time series. Otherwise the data series presents downward trend during the time period.

S5 BFAST algorithm

BFAST integrates the decomposition of time series into trend, seasonal, and remainder components with methods for detecting and characterizing abrupt changes within the trend and seasonal components[13]. BFAST can be applied to other disciplines dealing with seasonal or non-seasonal time series, such as hydrology, climatology, and econometrics[14].

$$Y_t = T_t + S_t + e_t, t = 1,2,3,\cdots,n \quad (5)$$

where Y_t is the observed data at time t, T_t is the trend component, S_t is the seasonal component, and e_t is the remainder component. It is assumed that T_t is piecewise linear, with break points $t_1^*, t_2^*, t_3^*, \cdots, t_m^*$ and define $t_0^*=0$, so that:

$$T_t = \alpha_j + \beta_j t \quad (6)$$

For $t_{j-1}^* < t \le t_j^*$ and where $j = 1,2,3,\cdots,m$. The intercept and slope of consecutive linear models, α_j and β_j, can be used to derive the magnitude and direction of the abrupt change (hereafter referred to as magnitude) and slope of the gradual change between detected break points. The magnitude of an abrupt change at a breakpoint is derived by the difference between T_t at t_{j-1}^* and t_j^*, so that:

$$Magnitude = (\alpha_{j-1} - \alpha_j) + (\beta_{j-1} - \beta_j)t \quad (7)$$

where the slopes of the gradual change before and after a break point are β_{j-1} and β_j.

S6 Relative contribution calculation

198 Stepwise Regression and Multiple linear regression (MLR) were used to establish the
199 relationship between sediment load and impact variables.

200 **Step1,** Stepwise regression was first used to fit sediment loads using many potential
201 independent variables as predictors, and the best subset was extracted from them for
202 use in your MLR model.

203 **Step2,** Relative contribution was calculated. The main steps were:

204 (1) Assume an $n\times1$ vector of criterion scores (y) and an $n\times p$ matrix of predictor
205 scores(X) of full rank, all of which are expressed in standard score form. If X has
206 at least as many as rows as columns, it is possible to find the singular value
207 decomposition of X ,

$$X = P\Delta Q', \tag{8}$$

$$\Delta = \sqrt{\text{eigenvalues}} \tag{9}$$

208 where, P and Q are contains the eigenvectors of XX' , and Δ is a diagonal
209 matrix containing the singular values of X .

210 (2) Find Z , which is the closest orthogonal matrix to X , $Z = PQ'$, Assume $X = \wedge Z$.

$$\wedge^{*} = \left(Z'Z\right)^{-1} Z'X = (QP'PQ')^{-1}QP'P\Delta Q' = Q\Delta Q', \tag{10}$$

211 (3) Calculate the part where y is interpreted by Z ,

$$\beta^{*} = \left(Z'Z\right)^{-1} Z'y = (QP'PQ')QP'y = QP'y, \tag{11}$$

212 where, β^{*} represent the proportion of predictable variance in y accounted for by
213 Z .

214 (4) Calculate the relative weight,

$$\omega = \frac{(\wedge^*)^2 \cdot \beta^*}{R^2} \times 100, \quad (12)$$

where, ω is the vector of relative weight and R^2 is R-square.

S7 B-spline curves

To reflect the changing shape and trajectory trend of the contribution rate of climate change and human activities to sediment transport, B-spline curves were used for fitting in this study. The B-spline curve equation can be expressed as:

$$P(u) = \sum_{i=0}^{n} P_i B_{i,k}(u) \quad u \in [u_{k-1}, u_{n+1}] \quad (13)$$

$$B_{i,k}(u) = \frac{u - u_i}{u_{i+k-1} - u_i} \times B_{i,k-1}(u) + \frac{u_i - u}{u_{i+k} - u_{i+1}} \times B_{i+1,k+1}(u) \quad (14)$$

$$B_{i,1}(u) = \begin{cases} 1, u_i \le u \le u_{i+1} \\ 0, otherwise \end{cases}, \quad define \frac{0}{0} = 0 \quad (15)$$

Where P_i is the control vertex, $B_{i,k}(u)$ (i = 0, 1 … n) is the k degree gauge B-spline basis function, i is the node number, the node vector u is distributed, equidistant along the parameter axis.

REFERENCES

1. Xu, Y., Xu, X. & Tang, Q. Human activity intensity of land surface: Concept, methods and application in China. *J. Geogr. Sci.* **26**, 1349–1361 (2016).

2. Luo, K. Response of hydrological systems to the intensity of ecological

engineering. *J. Environ. Manage.* **296**, 113173 (2021).

3. Moriasi, D. N. *et al.* Model Evaluation Guidelines for Systematic Quantification of Accuracy in Watershed Simulations. *Trans. ASABE* **50**, p.885-900 (2007).

4. Su, B. *et al.* Drought losses in China might double between the 1.5 °C and 2.0 °C warming. *Proc. Natl. Acad. Sci.* 201802129 (2018) doi:10.1073/pnas.1802129115.

5. Warszawski, L. *et al.* The inter-sectoral impact model intercomparison project (ISI-MIP): Project framework. *Proc. Natl. Acad. Sci. U. S. A.* **111**, 3228–3232 (2014).

6. Chu, Q., Xu, Z., Liu, W. & Liu, L. Assessment on 24 global climate models in the CMIP5 over the Yangtze River(in Chinese). *Resour. Environ. Yangtze Basin* **24**, 81–89 (2015).

7. Kubiszewski, I., Costanza, R., Anderson, S. & Sutton, P. The future value of ecosystem services: Global scenarios and national implications. *Ecosyst. Serv.* **26**, 289–301 (2017).

8. Peng, T. *et al.* Quantitative assessment of drivers of sediment load reduction in the Yangtze River basin, China. *J. Hydrol.* **580**, 124242 (2020).

9. Kendall, M. G. & Gibbons, J. D. Rank correlation methods. Ed. *Edward Arnold* (1990).

10. Kendall, M. G. Further contributions to the theory of paired comparisons.

Biometrics **11**, 43–62 (1955).

11. Mann, H. B. Nonparametric tests against trend. *Econom. J. Econom. Soc.* 245–259 (1945).

12. Li, B. *et al.* Eco-environmental impacts of dams in the Yangtze River Basin, China. *Sci. Total Environ.* **774**, 145743 (2021).

13. Verbesselt, J., Hyndman, R., Newnham, G. & Culvenor, D. Detecting trend and seasonal changes in satellite image time series. *Remote Sens. Environ.* **114**, 106–115 (2010).

14. Verbesselt, A. J. Package ‘ bfast ’. 1–8 (2011).